Title: Structure-function investigations of a stereospecific carboxyl esterase from *Bacillus coagulans*: non-lipase activities yet a lipase-like fold.

Valerio De Vitis[1], Cristina Nakhnoukh[2], Andrea Pinto[1], Martina Letizia Contente[1,3], Alberto Barbiroli[1], Mario Milani[4], Martino Bolognesi[2,5], Francesco Molinari[1], Louise J. Gourlay[2*] and Diego Romano[1*].

Affiliations:

[1] Department of Food, Environmental and Nutritional Sciences (DeFENS), Università degli Studi di Milano, Milano, Italy

[2] Department of Biosciences, Università degli Studi di Milano, Milano, Italy

[3] School of Chemistry, University of Nottingham, University Park, Nottingham, UK

[4] Biophysics Institute, National Research Council c/o Department of Biosciences, Università degli Studi di Milano, Via Celoria 26, 20133 Milano, Italy.

[5] Pediatric Research Center "Romeo ed Enrica Invernizzi", Cryo Electron Microscopy Laboratory, University of Milano, Milano, Italy

[*] Joint corresponding authors

Correspondence:

Louise J. Gourlay, Department of Biosciences, Università degli Studi di Milano, Via Celoria 26, Milano, 20133, Italy

Fax: +39 02 50314895

Tel: +39 02 50314914

E-mail: louise.gourlay@unimi.it

Diego Romano, Department of Food, Environmental and Nutritional Sciences (DeFENS), Università degli Studi di Milano, Via Mangiagalli 25, Milan, Italy

Fax: +39 02 50319238

Tel: +39 02 50319134

E-mail: diego.romano@unimi.it

Running title: Structure-function studies of stereoselective BCE

Abbreviations: BCE, *Bacillus coagulans* carboxylesterase 1; CD, circular dichroism; EtOAc, ethyl

acetate; hMGL, human monoglyceride lipase; IPG, 1,2-*O*-isopropylidenglycerol; pNPA, *p*-nitrophenyl acetate.

Keywords: carboxylesterase; IPG; *Bacillus coagulans*; crystal structure; lipase, enantioselective.

Database: Coordinates and structure factors have been deposited in the Protein Data Bank (www.rcsb.org) under accession numbers 5O7G (apo-BCE) and 5OLU (glycerol-bound BCE).

Conflicts of Interest: The authors declare that there are no conflicts of interest.

Abstract

Microbial carboxylesterases are important biocatalysts that selectively hydrolyze an extensive range of chiral and prochiral esters. Here, we report the recombinant preparation, biophysical and biochemical characterization of an atypical carboxylesterase from *Bacillus coagulans* (BCE), endowed with high enantioselectivity towards different 1,2-*O*-isopropylideneglycerol (IPG or solketal) esters. BCE efficiently catalyzes the production of enantiopure (*S*)-IPG, a chiral building block for the synthesis of β-blockers, glycerophospholipids and prostaglandins; efficient hydrolysis was observed up to 65°C. To gain insight into the mechanistic bases of such enantioselectivity, we solved the crystal structures of BCE in apo- and glycerol-bound forms at resolutions of 1.9 Å and 1.8 Å, respectively. *In silico* docking studies on the BCE structure confirmed our experimental data, showing that only IPG esters with small acyl chains (<C6) may be hydrolyzed and suggest that enantioselectivity may be due to an improved stabilization of the tetrahedral reaction intermediate for the *S*-enantiomer. In contrast to our data implying non-lipolytic functions, BCE displays a lipase-like structural feature- a so-called 'lid domain that caps the main entrance to the active site; in lipases the lid mediates catalysis by a process called interfacial activation; a phenomenon that we did not observe for BCE activity.

Overall, we investigate the functional-structural properties of an atypical carboxyl esterase that has non-lipase like functions, yet possesses a lipase-like 3D fold, in the context of utilizing BCE as an inexpensive, efficient biocatalyst for the industrial production of enantiopure (*S*)-IPG.

Introduction

Carboxylester hydrolases (EC 3.1.1.1) are enzymes that catalyze the cleavage and formation of carboxyl ester bonds, being often classified as esterases and lipases, based on experimental data and theoretical hypotheses. Recently, it has been suggested to simply organize carboxylester hydrolases into lipolytic esterases (proposed EC: L3.1.1.1) and non-lipolytic esterases (NLEst, proposed EC: NL3.1.1.1) [1], however they have also been classified, based on their sequence similarity and secondary structure conservation, taking advantage of databases, such as the Lipase Engineering Database (LED), the α/β-hydrolase Fold Enzyme Family 3DM or ESTHER [2-4]. Lipolytic esterases and non-lipolytic esterases are useful biocatalysts, especially for the (stereo)selective hydrolysis or synthesis of chiral and prochiral esters for the preparation of chiral drugs and their intermediates [5-7].

Bacteria belonging to the genus *Bacillus* are known producers of stereoselective carboxylesterases [8]. Lipolytic and non-lipolytic esterases from *B. subtilis* [9-14], *B. coagulans* [15], *B. amyloliquefaciens* [16], *B. stearothermophilus* [17], and generic *Bacillus* sp. [18] have been identified as excellent biocatalysts for the stereoselective hydrolysis of chiral and prochiral esters. This feature allows for the preparation of structurally different alcohols and carboxylic acids as single enantiomers.

Significant attention has been dedicated to the enantioselective hydrolysis of racemic esters of 1,2-*O*-isopropylideneglycerol (IPG or solketal) catalyzed by carboxylesterases, for the preparation of optically pure IPG [9, 15, 19-24]. Enantiopure IPG is an inexpensive and valuable chiral building block for the synthesis of β-blockers, glycerophospholipids, and prostaglandins [25]. However, enantioselective hydrolysis of IPG esters is difficult to obtain with lipolytic esterases (lipases); in a systematic study using commercial lipases, the best result was found with Amano AK lipase (from *Pseudomonas* sp.), which hydrolyzed (*R,S*)-IPG octanoate with good enantioselectivity, but with low yields (22% after 48 h) [25]. Other lipases, including *Candida antartica* lipase B (Novozyme 435), were poorly enantioselective towards acetate and octanoate IPG [26].

We previously identified and purified a carboxylesterase from *B. coagulans* (BCE) with medium-to-high enantioselectivity towards different racemic esters [27], including esters of IPG [5, 4]. The attractive thermophilic and stereoselective properties led us to further investigate this enzyme from both a biochemical and structural point-of-view as a potential target for industrial applications.

In this context, we present the high resolution (1.8-1.9 Å) crystal structures of BCE, solved in its apo-form and in complex with glycerol. Our functional studies demonstrate that BCE

functions as a non-lipolytic carboxylesterase and hydrolyzes C2-C8 esters, with maximum activity towards caproate (C6) esters, and can catalyze the production of optically pure (*S*)-IPG from racemic mixtures of butyrate and benzoate IPG esters. BCE is active at reaction temperatures as high as 65°C, showing typical Michaelis-Menten kinetics and has no apparent requirement for interfacial activation. This latter observation, and such non-lipase-like functions, contrasts structural observations that highlight the presence of a particularly large, lipase-specific lid domain that typically mediates interfacial activation. Here structural analyses of a lipase-like BCE are presented in relation to its non-lipolytic catalytic function and stereoselectivity for butyrate and benzoate IPG esters.

Results

Production of recombinant BCE

The gene coding for BCE (accession number WP_029142894) was amplified from *B. coagulans* NCIMB 9365 genomic DNA and cloned into the pET100/D-TOPO® bacterial expression vector. N-terminal His-tagged BCE fusion protein was produced in *Escherichia coli* BL21(DE3)Star cells, as described in the Experimental Procedures. Expression levels were determined by SDS-PAGE (data not shown) and by measuring enzyme activity (U/mg), monitoring the conversion of *p*-nitrophenyl acetate (pNPA) to *p*-nitrophenol. The highest specific activity was measured after induction with 0.5 mM IPTG for 16 h at 20°C in Luria-Bertani (LB) broth.

BCE was purified by affinity chromatography and exchanged into 50 mM Tris-HCl pH 8.0, 100 mM NaCl for activity assays, as described in the Experimental Procedures. BCE migrated on a 11% polyacrylamide gel at a molecular weight of 50 kDa, consistent with the calculated molecular mass of the full-length protein (39.2 kDa) plus the N-terminal His-tag (8.8 kDa). Under optimized conditions, 20 mU/mg of BCE was obtained, corresponding to a volumetric productivity of approximately 350 mU/L culture and to a specific productivity of 80 mU/g wet biomass.

BCE activity and enantioselectivity

BCE exhibited high activity towards *p*NPA between 45 and 65°C in 50 mM Tris-HCl pH 8.0 containing 100 mM NaCl; the highest activity was observed at 65°C. BCE was active at a pH range from 7.0 to 9.0.

The ability to hydrolyze substrates with longer acyl chains was investigated using *p*-nitrophenyl butyrate (C4), caproate (C6), caprylate (C8), caprate (C10), laurate (C12), and palmitate (C16) (**Figure 1**). BCE showed typical non-lipolytic behavior, being able to hydrolyze C2-C8 esters

following typical Michaelis-Menten kinetics, with a maximum activity towards caproate ester (see **Table 1** for kinetics data), whereas no activity was detected towards laurate and palmitate esters. The absence of interfacial activation was also confirmed by measuring the activity of BCE over a range of tributyrin concentrations (0.1-2.0 mM).

The enantioselectivity of the purified recombinant BCE was assayed using three different IPG esters (acetate, butyrate, and benzoate; **Table 2**), previously tested with the wild-type enzyme [14]. Hydrolysis of butyrate and benzoate esters occurred with high reaction rates and enantioselectivity (**Table 2**), whereas the biotransformation of acetate ester was much slower and less enantioselective. Biotransformation of IPG benzoate was carried out also on semi-preparative scale (200 mL), confirming the results obtained on small scale and proving the applicability of recombinant BCE as a preparative biocatalyst.

The 3D structure of BCE

The 3D structures of ligand-free BCE and glycerol-bound BCE were solved using X-ray diffraction data collected on single hexagonal (space group $P6_322$) crystal (per dataset) at resolutions of 1.9 Å and 1.8 Å, respectively, as described in the Experimental Procedures (**Figures 2A-C**). For both datasets, one BCE monomer was present in the asymmetric unit, with an estimated *w/v* solvent content of 63.1% (Matthews coefficient of 3.3 $Å^3$/Da). Interestingly, the molecular replacement package BALBES revealed that the hexagonal BCE unit cell (a=138.1 Å, b=138.1 Å, c= 83.3 Å) is identical to that of a eukaryotic polyphosphate polymerase in complex with orthophosphate (PDB entry 3G3T); this is a coincidence since the two enzymes are completely unrelated. Both BCE structures were refined to satisfactory R_{free} and R_{gen} values (**Table 3**). Electron density was well-defined for almost all of the BCE polypeptide, except for the last C-terminal residue and include an additional residue (in glycerol-bound BCE) or two (for ligand-free BCE) extra residues at the N-terminus that pertain to the cloning region of the pET100/D-TOPO bacterial expression vector.

Overall 3D Fold

The overall 3D fold of both BCE structures are essentially identical (*rmsd* value 0.3 Å), displaying the canonical α/β hydrolase fold shared by all members of this superfamily. The central β-sheet comprises seven parallel strands (β1 and β3-8) and one anti-parallel β-strand (β2) inserted between β-strands 1 and 3, and contains eleven α-helices and two 3_{10} α-helices (**Figure 2A**). In contrast to activity studies, which suggest that BCE is a non-lipolytic carboxylesterase, BCE presents a lipase-like 3D fold deduced by the presence of an extra so-called 'lid domain', comprising three α-helices

(α5, α6 and α8) that caps the entrance to the active site, housed in the canonical α/β hydrolase core (**Figure 2A**).

Accordingly, despite poor sequence conservation (25.1% sequence identity), the closest structural homolog (*rmsd* value of 1.72 Å over 154/304 Cα pairs) to BCE is human monoglyceride lipase (hMGL; PDB entry 3JWE [28]), as determined using Profunc (http://www.ebi.ac.uk/thornton-srv/databases/profunc/); structural conservation resides almost entirely in the α/β-hydrolase domain and the lid domains differ significantly (**Figure 2D**). hMGL, like all mono- and diacylglycerol lipases studied to date, belongs to the single α-helix/loop lid lipase class [29]. If BCE were it in fact a true lipase, it would pertain to the large-lid class characteristic of thermophilic lipases, however in light of our activity data, it is likely that BCE belongs to an entirely different carboxyl esterase class all together. Additional structural differences between the two proteins occur at the N-terminus; hMGL contains an extra α-helix, a shorter β-strand 1, and α2 in BCE is replaced by an unstructured loop in hMGL (**Figure 2D**).

The BCE lid domain

As previously mentioned, the absence of interfacial activation for catalysis is contradictory to the presence of the lipase-specific lid-domain that mediates this process. The BCE lid domain (residues 145-235) is particularly large, also with respect to the lids of the 21 other lipase members (of known structure) belonging to the large lid lipase subclass [29]. Open and closed lid conformations have been crystallized for several lipases, however the BCE lid was found in the closed conformation in all datasets collected to date, despite the absence or presence of glycerol bound at the active site (**Figure 2B**). Only two lid residues (F209 and T210), housed in a 11-residue loop that connects α7 and α8 and forms the entrance to the active site, are diversely positioned. Interestingly in apo-BCE, lid closure does not completely block entrance to the active site, and an aperture with diameter of approximately 13 Å is visible (**Figure 3A**). This aperture may permit the diffusion of small substrates directly into the active site without requiring lid repositioning. In the glycerol-bound enzyme, the repositioning of F209 and T210 is sufficient to partially close the active site aperture.

The presence of an active site aperture and the lack of classical lipolytic carboxylesterase activity, however, does not rule out the possibility of the BCE lid switching between open and closed conformations during catalysis. Accordingly, molecular dynamics calculations were made using the online server PiSQRD (http://pisqrd.escience-lab.org) to assess BCE lid flexibility. Glycerol-free BCE was fragmented by computational simulations into two domains that can behave as rigid units, moving independently from one another during protein structural fluctuations (in conditions of thermal equilibrium); the two domains (residues 78 to 85 (domain 1) and residues

143-227 (domain 2)) essentially represent the core α/β-hydrolase domain and the lid domain, thus highlighting the potential dynamical role of this region of the protein [31].

The BCE active site

The BCE active site contains a conserved catalytic triad (S114, H284 and D251) with the catalytic S114 being housed in the conserved GXSXG (GSHMG in BCE) motif on β5 that represents the nucleophilic elbow hosted in a turn that links β5 and α4. The oxyanion hole, which stabilizes the anionic transient tetrahedral intermediate of catalysis, is built by the backbone NH groups of M115 and G116 of the nucleophilic elbow, and by residues G37 (Cα) and F38 (side-chain atoms). The active site-bound glycerol molecule observed in several of the analyzed crystals hydrogen-bonds with glycerol atom O2 and a water molecule that also interacts with the hydroxyl group of S114 and, via glycerol atom O1 with adjacent residues H113(NE2), and E285(OE2) (**Figure 2D**).

Surface cavity analysis using CAST-P (www. http://sts.bioe.uic.edu/castp/) and the atomic coordinates of apo-BCE, revealed the solvent-accessible active site cavity (volume = 752.3 $Å^3$; area= 877.7 $Å^2$), which comprises main-chain and/or side chain atoms of 34 residues (**Figure 3A**) [31]. In glycerol-bound BCE, the size of this cavity increases (volume = 1028.6 $Å^3$; area= 1370.2 $Å^2$), however solvent accessibility decreases due to slight closure of the aperture to the active site due to the repositioning of residues F209 and T210.

***In silico* docking of tested IPG ester substrates**

The BCE active site is accessible by a wide tunnel terminating in a hydrophobic cavity located after the active residue Ser114 (**Figure 3A**), lined by hydrophobic residues: M118, F143, L173, M174, M177, F221, M225. The hydrophobic cavity is quite short (~ 10 Å) and thus unable to host large aliphatic chains; this explains why BCE is inactive with compounds longer than C10 (as previously shown in **Figure 1**). Analysis by *in silico* docking, using *p*-nitrophenyl compounds with different acyl chains, shows that molecules from C2 to C6 can dock into the cavity in conformations compatible with observed enzymatic activity (**Figure 3B**). On the contrary, the hydrophobic cavity is too short to host compounds bigger than C6 in their correct conformations. It is possible that the high temperature required for optimal enzymatic activity induces some structural rearrangements that allow molecules up to C10 to be processed.

We subsequently used *in silico* docking to try to gain insight into the structural bases of the enantioselectivity of BCE. The calculated dissociation constants (K_d) for *R* and *S* enantiomers of different IPG esters (acetate, butyrate, and benzoate) are quite similar (**Table 4**), and thus does not explain the enantioselectivity observed in the experiments. To further investigate this question, the

overall geometry of the chiral ligands in the active site was analyzed and found to differ, and can at least partially explain the different reaction efficiencies toward *R* or *S*-enantiomers. Among others, a parameter that is important for the enzymatic activity is the distance between the oxygen of the alcohol moiety of the esters and H284 (see **Table 4** and **Figure 3C**). This distance is crucial to stabilize the tetrahedral intermediate (Step 2) formed during the reaction, as previously described [33]. In IPG acetate, the H284 distance from the oxygen of the alcohol moiety in both *R*- and *S*-enantiomers is the same, in agreement with the lower level of discrimination. On the contrary, the distance is reduced from 5.0 Å to 4.3 Å for the *R*- and *S*-enantiomers of the butyrate ester, respectively; this would suggest a higher efficiency in Step 2 towards *S*-enantiomers (**Figure 3C**). Overall, these observations imply that enantioselectivity may be due to a combination of different features, including the different permeation of the enantiomers toward the active site (selected by the access tunnel).

Circular dichroism and thermal stability studies

The conformational stability of BCE in solution was characterized by circular dichroism (CD). In agreement with the crystal structure, the far-UV CD spectrum shows the typical features of α-helix rich proteins: two minima at 220 and 208 nm, and an intersection at zero at about 203 nm (**Figure 4, inset**). Thus, the thermal stability of BCE was assessed in function of increasing temperature, monitoring the ellipticity at 220 nm (reporter of α-helix secondary structures) as described in the Experimental Procedures.

The BCE melting curve is biphasic, with a first minor conformational transition at 42°C (T_{m1}, 30% of the total transition) and a second main transition at 87°C (T_{m2}, 70% of the total transition) (**Figure 4A**). The second transition triggers a macroscopic aggregation of unfolded protein that causes irreversible denaturation. The reversibility of the first transition was studied by setting-up a multistep temperature ramp experiment. A native BCE sample was heated in a first temperature ramp from 20 to 60°C and then cooled down to the starting temperature of 20°C. The same BCE sample was heated in a second temperature ramp up to 95°C (**Figure 4B**). In the second temperature ramp the first minor melting is no longer visible, whereas the second main transition is perfectly conserved, proving that the two transition are irreversible and, apparently, independent.

Although the structural regions involved in the first transition have not been identified, to gain better insight into the nature of these conformational transitions we carried-out activity assays on BCE, with and without heat-treatment at 60°C. Interestingly, after 30 min, also the heat-treated protein was catalytically competent, although a 90% decrease in activity was observed. According to the molecular dynamics calculations that divide the BCE structure into two independent domains

(the core α/β-hydrolase domain and the lid domain), we hypothesize that the lid domain may be responsible for the first unfolding event, affecting the catalytic function of BCE only marginally. This hypothesis is also in good agreement with a "quantitative" analysis of the unfolding trace: the signal lost in the first transition is about 30%, thus compatible with loss of the three α-helices of the lid relative to a total of the eleven α-helices of the whole structure. Lid unfolding would have an effect on binding to the hydrophobic tail of the substrate, whereas binding to the oxyanion hole would be essentially unaffected.

Protein thermostability can be attributed to a number of other structural features such as the presence of disulfide bonds and intra-helical salt bridges [33]. BCE1 does not contain any disulfide bonds and in fact, only contains one non-conserved cysteine residue (C137). Using the ESPRI web server (http://bioinformatica.isa.cnr.it/ESBRI/introduction.html), 21 salt bridges (2.4-3.9 Å) were found in BCE, none of which are present within the lid domain, although two are formed between lid residue (D79) and residues R14(NZ) (3.2 Å) and R216(NH2) (3.1 Å (OD2) and 3.3 Å (OD1)) [34, 35]. These analyses also corroborate the theory that the α/β-hydrolase core is stable to a greater extent than the lid domain, supporting both the MD and CD studies and reinforces the likelihood that lid unfolding is responsible for the first unfolding transition.

Discussion

Carboxylesterases are ubiquitous enzymes that catalyze the cleavage and/or formation of carboxyl ester bonds. Their division into lipolytic (lipases) and non-lipolytic esterases is based on experimental data and theoretical hypothesis, and is often quite uncertain. All carboxylesterases share the so-called α/β hydrolase fold, where five (or more) strands in a central β-sheet forming the protein core are connected by α-helices; this superfamily is one of the largest families of structurally-related enzymes. Despite such elevated structural conservation, α/β-hydrolase members catalyze a wide variety of chemical transformations, and thus are extensively used in industrial processes. Lipases are characterized by the presence of a mobile subdomain (lid), which caps and shields substrate entry to the active site. The closed-lid conformation is supposed to be preponderant in water, where most lipases are poorly active, whereas interactions with hydrophobic compounds (substrates, organic solvents) are thought to prompt a conformational change of the lid making it accessible to the substrates (open-lid). The overall phenomenon is generally referred as "interfacial activation" [36].

Due to their advantageous biochemical properties, such as high chemo-, regio- and stereo-selectivity and thermostability, microbial carboxylesterases have numerous industrial applications in a wide range of sectors [4-6]. Kinetic resolution of racemic esters of chiral alcohols *via* their

enantioselective hydrolysis is among the most studied application. Optically pure (*S*)-1,2-O-isopropylideneglycerol (IPG) is a key intermediate for the preparation of β-blockers, leukotrienes, phospholipids, and prostaglandins [24]. Hydrolysis of racemic IPG esters has been explored using different carboxylesterases aiming at optically pure (*S*)-IPG; commercially available lipases are generally poorly active or scarcely enantioselective towards racemic IPG esters [25]. We previously found that BCE, a carboxylesterase from *B. coagulans,* carried out the kinetic resolution of different racemic IPG esters yielding (*S*)-IPG with high enantioselectivity [14].

To gain insight into the structure-function properties of BCE that may account for such enantioselectivity for IPG esters, we carried out the recombinant production, functional characterization and 3D structure determination of BCE (ligand-free and glycerol-bound). Recombinant BCE successfully catalyzed the enantioselective hydrolysis of different IPG esters in providing optically pure *(S)*-IPG with good reaction rates and excellent enantiomeric ratios; the best results being obtained with butyrate (C4) and benzoate (C6) IPG esters. Activity however diminished by 10% for C8 chains and by 90% for C10 chains and was completely abolished for C12 and C16 chains. In line with these data, structure analyses show that the active site cavity may only accommodate substrates with aliphatic carbon chain lengths shorter or equal to C6. Given the activity of BCE at elevated reaction temperatures that reach as high as 65°C, it is possible that at high temperatures, a conformational change is induced, allowing expansion of the active site and permitting the hydrolysis of slightly longer substrates. In fact, CD thermal stability studies show that there are two unfolding events, with the former occurring at a T_M of 45°C. We hypothesize that this event reflects the unfolding of the lid domain, as indicated by MD studies and structural observations made that underline the presence of 21 stabilizing salt bridges in the α/β-hydrolase core and none in the lid domain. Given that hydrophobic residues of the lid domain contribute to forming the hydrophobic cavity that binds the aliphatic carbon tail of ester substrates, it is unsurprising that substrate specificity may be altered at higher reaction temperatures.

Poor activity towards long-chain esters, together with IPG ester enantioselectivity are typical features of non-lipolytic carboxylesterases. Moreover, benzoate esters, the preferred substrate of BCE, are not preferred substrates for lipases (with the exception of the very versatile *Candida antartica* Lipase B-CALB) [37]. Such functional findings are in sharp contrast to our structural studies that highlight the presence of a lipase-typical lid domain, in addition to the canonical α/β-hydrolase fold. Given the role of this domain for catalysis in a process termed interfacial activation, where optimal reaction rates are observed at the hydrophobic-water interface, we carried out experiments in the presence of a triglyceride layer reproduced by the addition of tributyrin. In agreement with our activity studies but in contrast to the presence of this lipase-specific domain,

interfacial activation was not observed. The lack of interfacial activation and the fact that BCE was able to convert the (small) substrates used in this study in water with conventional kinetics, was also implied by the lack of lid positioning in the ligand-free and glycerol-bound structures. Interestingly, despite the observed 'closed' lid state of ligand-free BCE, access to the substrate-binding site was not completely blocked and a 13 Å mouth-opening to the active site tunnel was observed that could easily permit the diffusion of IPG esters, as illustrated by our structural analyses. Despite non-lipase functions, we cannot rule out the lid domain switching between 'open' and 'closed' conformations; *in silico* simulations and computational analyses carried out on the BCE structure, focusing on protein flexibility and rigid body movements, detected the lid domain as a mobile entity.

In lipases, the size and structural arrangement of the lid domain varies considerably and recent attempts have been made to classify lipase sub-groups according to the size and conformation of the lid [30]. Based on 44 distinct lipase structures, three lipase lid sub-groups were devised: *i)* lipases that lack a lid, *ii)* lipases that contain a lid formed by a single loop or α-helix, and *iii)* lipases that contain lids comprised of two or more α-helices. A link between optimum reaction temperature and lid organization was observed; large lids are correlated to increased catalysis at higher reaction temperatures [30]. Based on this classification, and the particularly large BCE lid (approx. 90 residues), were BCE an actual lipase, it would pertain to the third class of large lid lipases that exhibit thermostable properties (**Figure 3A**) [30]. This is in agreement with our findings, demonstrating that BCE remains active at high reaction temperatures.

Commentato [LG1]: visto che non è un lipase, forse non ha senso di aggiungere questo?

Our studies revealed that BCE is an atypical carboxylesterase characterized by non-lipolytic functionalities in contrast to a lipase-like 3D fold. With regards to the enantioselective hydrolysis of short-chain and benzoate esters of IPG, with a preference for *(S)*-IPG esters, *in silico* docking studies on the BCE structure suggest that a reduced distance between the catalytic histidine residue (H284) side chain that stabilizes the tetrahedral reaction intermediate during catalysis and the oxygen atom of the ester alcohol group, may play a role, however further studies are required. Thanks to the here-reported crystal structures, *in silico* docking may be used to identify inhibitors that may be used in co-crystallization studies to reveal the active residues that govern this specificity. Our results may pave the way for rational engineering strategies aimed at the construction of new variants with wider substrate specificities, and thus suited for different applications as stereoselective biocatalysts

Experimental Procedures

Production of recombinant BCE

The BCE gene coding for the full-length protein was amplified from *B. coagulans* genomic strain NCIMB 9365 DNA by PCR using the following primers: Forward: 5'-CACCATGTTGGCTTTTCAAGAGTTGAG-3'; Reverse: 5'-TGAGCTCGAGTCATTTTACGATGATCCCGTT-3'. The amplified gene was cloned into the pET100/D-TOPO® vector (Invitrogen) in frame with a N-terminal six-histidine tag, according to the manufacturer's instructions. Correct construct sequence was confirmed by DNA sequencing.

Cultures of BL21(DE3)Star *E. coli* cells were transformed with the resulting plasmid and grown overnight at 37 °C in LB medium supplemented with 100 mg/L ampicillin. The seed culture was then diluted into 1.0 L Erlenmeyer flasks containing 100 ml Luria Broth (LB) at an initial OD_{600nm} of 0.1. Cultivation was carried out at 37 °C with agitation at 150 rpm. Cells were grown until an OD_{600nm} of 0.8. After cold-shock treatment, cultures were induced with 0.5 mM IPTG (isopropyl- β-D-thiogalactopyranoside) and further incubated for 16 h at 20 °C. Bacterial cells were harvested by centrifugation at 5000 rpm for 15 min, washed once with 20 mM sodium phosphate buffer at pH 7.0 and stored at -20 °C.

The cell pellet was resuspended in 50 mM Tris-HCl pH 8.0 containing 100 mM NaCl, 6 mM imidazole. Bacterial cells were lysed by sonication (5 cycles of 30 s each, in ice, with 1 min interval) and the supernatant was harvested by centrifugation at 15,000 rpm for 45 min at 4 °C. BCE was purified from the supernatant by affinity chromatography with HIS-Select Nickel Affinity Gel (Sigma-aldrich) pre-equilibrated with 50 mM Tris-HCl pH 8.0, containing 100 mM NaCl, 6 mM imidazole. After a washing step with 50 mM Tris-HCl pH 8.0, 100 mM NaCl, 6 mM imidazole, His-BCE was eluted with 50 mM Tris-HCl pH 8.0, 100 mM NaCl, 250 mM imidazole.

For crystallization trials, BCE was purified from a 0.5L bacterial culture on a 5 ml Bio-scale Mini Profinity IMAC cartridge using the Profinia Protein Purification System (Bio-rad), following standard Bio-rad protocols. Purified BCE was exchanged into crystallization buffer (10 mM Tris-HCl pH 8.0; 150 mM NaCl) using a PD10 desalting column (GE Healthcare), according to the manufacturer's instructions and concentrated to 6.5 mg/ml, using an Amicon Ultra-15 centrifugal filter (Millipore) with a MW cut-off of 10 kDa.

Biotransformations of IPG esters

Biotransformations of IPG esters were carried out in 5 mL screw capped tube, using 7 mU of BCE in 1 mL of 50 mM Tris-HCl pH 8.0, 100 mM NaCl. The substrates were added at the final concentration of 5 mM, dissolved in DMSO at a final concentration of 0.5%. Incubations were carried out with magnetic stirring at 30°C. Conversions and stereochemical outcomes were monitored by gas chromatography using a chiral capillary column (diameter 0.25 mm, length 25 m,

thickness 0.25 µm, DMePeBeta-CDX-PS086, MEGA, Legnano, Italy) with a 0.25 mm-diameter, 25 m-length and 0.25 m-thickness, using the following temperature gradients: for IPG acetate: 10 min at 90 °C, increased to 120 °C over 15 min, maintained at 120 °C for 10 min and then increased to 180 °C over 2 min and then maintained at 180 for 10 min; for IPG butyrate: 10 min at 90 °C, increased to 110 °C over 5 min, maintained at 110 °C for 10 min and then increased to 180 °C over 2 min and then maintained at 180 for 10 min; for IPG benzoate: 10 min at 90 °C, increased to 120 °C over 3 min, maintained at 120 °C for 10 min and then increased to 180 °C over 2 min and then maintained at 180 for 10 min. Retention times of IPG enantiomers and esters under these conditions were: (*R*)-IPG= 8.2 min, (*S*)-IPG= 9.0 min; (*R*)-IPG acetate = 13.1 min, (*S*)-IPG acetate = 12.4 min; (*R*)-IPG butyrate =22.3 min, (*S*)-IPG butyrate = 21.2 min; (*R*)-IPG benzoate = 27.7 min, (*S*)-IPG benzoate = 27.5 min. Enantiomeric excesses (e.e.) were calculated using the following formulas: $e.e._{substrate}$ = ([(*S*)-IPG ester] - [(*R*)-IPG ester])/ ([(*S*)-IPG ester] + [(*R*)-IPG ester]) and $e.e._{product}$ = ([(*S*)-IPG] - [(*R*)-IPG])/ ([(*S*)-IPG] + [(*R*)-IPG])

Hydrolysis of IPG benzoate was also performed on semi-preparative scale: 250 mg (1.06 mmol) of substrate were dissolved in DMSO (1 mL) and added to 199 mL of 50 mM Tris-HCl pH 8.0, containing 100 mM NaCl. Upon addition of BCE (7 mU mL^{-1}), the reaction was followed by gas-chromatography and stopped after 50 min (in correspondence to a 60% conversion). The reaction was stopped by adding 100 mL ethyl acetate (EtOAc) to recover both unreacted (*S*)-IPG benzoate and enantiomerically pure (*S*)-IPG. The aqueous phase was extracted by repeating the addition of EtOAc twice. Organic extracts were collected, dried over sodium sulfate and the solvent removed under reduced pressure. Flash chromatography (*n*-hexane/EtOAc, 75/25) on silica gel pretreated with triethylamine afforded 52 mg of optically pure (*S*)-IPG (ee > 99% by chiral GC).

Activity and kinetic analyses of BCE activity

Kinetic parameters were measured spectrophotometrically using different concentrations of *p*-nitrophenyl esters (actetate, butyrate, caproate, caprylate, laurate, and palmitate) at 28°C in 1 mL of 50 mM Tris-HCl pH 8.0, NaCl 100 mM (final 0.3% acetone), monitoring the increase of absorbance at 400 nm due to the production of *p*-nitrophenol (15000 $M^{-1}cm^{-1}$). Experimental data were fitted to suitable kinetic models with Origin 9.0 and kinetic parameters (V_{max}, K_m) were calculated with the same program. BCE activity (0.036 mg mL^{-1}) was routinely measured spectrophotometrically using 0.015 mM *p*-NPA as a substrate, following the reaction for 5 min. One unit of BCE corresponds to the amount of protein that produces 1 µmol of *p*-nitrophenol in 1 min. Hydrolysis of tributyrin (in the range of 0.1-2.0 mM) was measured titrimetrically at 37 °C with a pH-stat using 30 mL phosphate buffer (10 mM pH 7.0) (.

BCE crystallization

Crystallization trials of BCE (6.5 mg/ml) were prepared in 96-flat well sitting drop plates (Greiner), containing 100 μL crystallization solution of PACT Premier™Crystallization screen (Molecular Dimensions). 400 nL drops were deposited at diverse protein concentrations (30, 50 and 70 % of the stock protein solution) and crystals grew after approximately 1 week in several conditions. Data for the apo-enzyme were collected on a single crystal grown in condition 2-11 (20% PEG3350; 0.1 M sodium citrate tribasic hydrate); the crystal was cryoprotected in 50% PEG3350. Data for the glycerol-bound form of BCE were collected on a single crystal grown in condition 42 (1.5 M ammonium sulfate, 12% glycerol and 0.1 M Tris-HCl, pH 8.0) of Hampton Crystal Screen II (Hampton Research). For cryoprotection the concentration of glycerol was raised to 25%.

Data Collection, model building and refinement

X-ray diffraction Data were collected at the ID29 (glycerol-bound enzyme), ID23-1 (apo-enzyme) beamlines at the European Synchrotron Radiation Facility (ESRF, Grenoble, France). Data were processed using XDS and assigned to the hexagonal $P6_322$ space group using POINTLESS and scaled using AIMLESS, available in the CCP4i suite [38-40]. The 3D structure of BCE was solved *via* molecular replacement using BALBES and the protein sequence as the input; the BALBES search model was based on the structure of human monoglyceride lipase (PDB entry 3PE6) [28, 41]. The initial model was refined with PHENIX.refine, including a translational-libration-screw (TLS) option, final R_{gen} and R_{free} values of 21 and 24.3% (apo-BCE) and 14.7 and 16.9% (glycerol-bound BCE) were reached, respectively (**Table 3**). Both final models present ideal geometric parameters, with 97.7% (apo-BCE) and 98.1% (glycerol-bound BCE) residues assigned to the most favorable regions of the Ramachandran plot, with no outliers, according to structure validation using MolProbity under the Phenix platform (**Table 3**).

Circular dichroism

CD measurements were performed with a J-810 spectropolarimeter (JASCO Corp., Tokyo, Japan) equipped with a Peltier system for temperature control. All measurements were performed in crystallization buffer (10 mM Tris-HCl pH 8, 150 mM NaCl) at a protein concentration of 0.2 mg/ml, and in a 0.1 cm path length cuvette. Temperature ramps experiments were monitored at a wavelength of 220 nm (temperature slope 1°C/min). T_ms were calculated as the maximum of the first-derivative of the traces.

Acknowledgements

LJG and DR gratefully acknowledge departmental Università degli Studi di Milano 'Linea 2' funding.

Author contributions

VdV and DR designed and performed the experiments involving the preparation and purification of the recombinant enzymes. AP and MLC synthesized all substrates and optimized the analytical conditions. VdV and DR performed all the experiments of enzyme characterization and biotransformations. FM and MB analyzed the data, and wrote the manuscript. AB performed the CD experiments and wrote the manuscript. CN and LJG carried out purification, crystallization and 3D structure analyses. MM carried out *in silico* docking, related structural analyses and wrote the related section. DR and LJG coordinated the work and wrote the manuscript.

References

1. Ali, Y. B., Verger, R. & Abousalham, A. (2012) Lipases or esterases: does it really matter? Toward a new bio-physico-chemical classification, *Methods in molecular biology.* **861**, 31-51.

2. Fischer M., Pleiss J. (2003) The Lipase Engineering Database: a navigation and analysis tool for protein families. *Nucleic acids research.* **31**, 319-321.

3. Hotelier, T., Renault, L., Cousin, X., Negre, V., Marchot, P. & Chatonnet, A. (2004) ESTHER, the database of the alpha/beta-hydrolase fold superfamily of proteins, *Nucleic acids research.* **32**, D145-7.

4. Kourist, R., Jochens, H., Bartsch, S., Kuipers, R., Padhi, S. K., Gall, M., Bottcher, D., Joosten, H. J. & Bornscheuer, U. T. (2010) The alpha/beta-hydrolase fold 3DM database (ABHDB) as a tool for protein engineering, *Chembiochem : a European journal of chemical biology.* **11**, 1635-43.

5. Carvalho, A. C., Fonseca Tde, S., de Mattos, M. C., de Oliveira Mda, C., de Lemos, T. L., Molinari, F., Romano, D. & Serra, I. (2015) Recent Advances in Lipase-Mediated Preparation of Pharmaceuticals and Their Intermediates, *International journal of molecular sciences.* **16**, 29682-716.

6. Romano, D., Bonomi, F., de Mattos, M. C., de Sousa Fonseca, T., de Oliveira Mda, C. & Molinari, F. (2015) Esterases as stereoselective biocatalysts, *Biotechnology advances.* **33**, 547-65.

7. Gotor-Fernandez, V., Brieva, R and Gotor, V (2006) Lipases: Useful biocatalysts for the preparation of pharmaceuticals., *J Mol Catal.* **40**, 111-120.

8. Guncheva, M., Zhiryakova, D. (2011) Catalytic properties and potential applications of Bacillus lipases., *J Mol Catal.* **B68**, 1-21.

9. Droge, M. J., Bos, R. & Quax, W. J. (2001) Paralogous gene analysis reveals a highly enantioselective 1,2-O-isopropylideneglycerol caprylate esterase of Bacillus subtilis, *European journal of biochemistry.* **268**, 3332-8.

10. Quax, W. J. & Broekhuizen, C. P. (1994) Development of a new Bacillus carboxyl esterase for use in the resolution of chiral drugs, *Applied microbiology and biotechnology.* **41**, 425-31.

11. Rozeboom, H. J., Godinho, L. F., Nardini, M., Quax, W. J. & Dijkstra, B. W. (2014) Crystal structures of two Bacillus carboxylesterases with different enantioselectivities, *Biochimica et biophysica acta.* **1844**, 567-75.

12. Schmidt, M., Henke, E., Heinze, B., Kourist, R., Hidalgo, A. & Bornscheuer, U. T. (2007) A versatile esterase from Bacillus subtilis: cloning, expression, characterization, and its application in biocatalysis, *Biotechnology journal.* **2**, 249-53.

13. Steenkamp, L., Brady, D. (2008) Optimisation of stabilised carboxylesterase NP for enantioselective ester hydrolysis of naproxen methyl ester., *Process Biochem.* **43**, 1419-26.

14. van Pouderoyen, G., Eggert, T., Jaeger, K. E. & Dijkstra, B. W. (2001) The crystal structure of Bacillus subtilis lipase: a minimal alpha/beta hydrolase fold enzyme, *Journal of molecular biology.* **309**, 215-26.

15. Molinari, F., Brenna, O., Valenti, M., Aragozzini, F. (1996) Isolation of a novel carboxylesterase from Bacillus coagulans with high enantioselectivity toward racemic esters of 1,2-O-isopropylideneglycerol., *Enzyme Microb Technol.* **19**, 551-6.

16. Liu, J. Y., Zheng G.W., Imanaka, T, Xu J.H. (2014) Stepwise and combinatorial optimization of enantioselectivity for the asymmetric hydrolysis of 1-(3',4'-methylenedioxyphenyl)ethyl acetate under use of a cold-adapted Bacillus amyloliquefaciens esterase, *Biotechnol Bioprocess Eng.* **99**, 442-8.

17. Henke, E. & Bornscheuer, U. T. (2002) Esterases from Bacillus subtilis and B. stearothermophilus share high sequence homology but differ substantially in their properties, *Applied microbiology and biotechnology.* **60**, 320-6.

18. Fillat, A., Romea, P., Urpi, F., Pastor, F. I. & Diaz, P. (2014) Improving enantioselectivity towards tertiary alcohols using mutants of Bacillus sp. BP-7 esterase EstBP7 holding a rare GGG(X)-oxyanion hole, *Applied microbiology and biotechnology.* **98**, 4479-90.

19. Godinho, L. F., Reis, C.R., van Merkerk R., Poelarends G-L., Quax W.J. (2012) An esterase with superior activity and enantioselectivity towards 1,2-O-isopropylideneglycerol esters obtained by protein design., *Adv Synth Catal.* **354**, 3009-15.

20. Godinho, L. F., Reis, C. R., Rozeboom, H. J., Dekker, F. J., Dijkstra, B. W., Poelarends, G. J. & Quax, W. J. (2012) Enhancement of the enantioselectivity of carboxylesterase A by structure-based mutagenesis, *Journal of biotechnology.* **158**, 36-43.

21. Godinho, L. F., Reis, C. R., Tepper, P. G., Poelarends, G. J. & Quax, W. J. (2011) Discovery of an Escherichia coli esterase with high activity and enantioselectivity toward 1,2-O-isopropylideneglycerol esters, *Applied and environmental microbiology.* **77**, 6094-9.

22. Molinari, F., Romano, D., Gandolfi, R., Kroppenstedt, R. M. & Marinelli, F. (2005) Newly isolated Streptomyces spp. as enantioselective biocatalysts: hydrolysis of 1,2-O-isopropylidene glycerol racemic esters, *Journal of applied microbiology.* **99**, 960-7.

23. Monti, D., Ferrandi, E. E., Righi, M., Romano, D. & Molinari, F. (2008) Purification and characterization of the enantioselective esterase from Kluyveromyces marxianus CBS 1553, *Journal of biotechnology.* **133**, 65-72.

24. Romano, D., Falcioni, F, Mora, D. and Molinari, F. (2005) Enhanced enantioselectivity of Bacillus coagulans in the hydrolysis of 1,2-O-isopropylidene glycerol esters by thermal knock-out of undesired enzymes, *Tetrahedron Asymmetry.* **16**, 841-5.

25. Jurczac, J., Pikul, S., Bauer, T., (1986) *Tetrahedron Asymmetry.* **42**, 447-488.

26. Machado, A., da Silva, A., Borges, C., Simas, A, Freire, D. (2011) Kinetic resolution of (R,S)-1,2-isopropylidene glycerol (solketal) ester derivatives by lipases, *Journal of Molecular Catalysis B: Enzymatic* **69**, 42-46.

27. Romano, A., Romano, D, Molinari, F, Gandolfi, R & Costantino, F (2005) A new chemoenzymatic synthesis of D-cloprostenol. , *Tetrahedron: Asymmetry* **16**, 3279-3282.

28. Schalk-Hihi, C., Schubert, C., Alexander, R., Bayoumy, S., Clemente, J. C., Deckman, I., DesJarlais, R. L., Dzordzorme, K. C., Flores, C. M., Grasberger, B., Kranz, J. K., Lewandowski, F., Liu, L., Ma, H., Maguire, D., Macielag, M. J., McDonnell, M. E., Mezzasalma Haarlander, T., Miller, R., Milligan, C., Reynolds, C. & Kuo, L. C. (2011) Crystal structure of a soluble form of human monoglyceride lipase in complex with an inhibitor at 1.35 A resolution, *Protein science : a publication of the Protein Society.* **20**, 670-83.

29. Bertrand, T., Auge, F., Houtmann, J., Rak, A., Vallee, F., Mikol, V., Berne, P. F., Michot, N., Cheuret, D., Hoornaert, C. & Mathieu, M. (2010) Structural basis for human monoglyceride lipase inhibition, *Journal of molecular biology.* **396**, 663-73.

30. Khan, F. I., Lan, D., Durrani, R., Huan, W., Zhao, Z. & Wang, Y. (2017) The Lid Domain in Lipases: Structural and Functional Determinant of Enzymatic Properties, *Frontiers in bioengineering and biotechnology.* **5**, 16.

31. Pettersen, E. F., Goddard, T.D., Huang, C.C., Couch, G.S., Greenblatt, D.M., Meng, E.C., Ferrin, T.E. (2004) UCSF Chimera--a visualization system for exploratory research and analysis. , *J Comput Chem.* **25**, 1065-12.

32. Aleksiev, T., Potestio, R., Pontiggia, F., Cozzini, S. & Micheletti, C. (2009) PiSQRD: a web server for decomposing proteins into quasi-rigid dynamical domains, *Bioinformatics.* **25**, 2743-4.

33. Dundas, J., Ouyang, Z., Tseng, J., Binkowski, A., Turpaz, Y. & Liang, J. (2006) CASTp: computed atlas of surface topography of proteins with structural and topographical mapping of functionally annotated residues, *Nucleic acids research.* **34**, W116-8.

34. Kumar, S., Tsai, C. J., Ma, B. & Nussinov, R. (2000) Contribution of salt bridges toward protein thermostability, *Journal of biomolecular structure & dynamics.* **17 Suppl 1**, 79-85.

35. Kumar, S. & Nussinov, R. (1999) Salt bridge stability in monomeric proteins, *Journal of molecular biology.* **293**, 1241-55.

36. Reis, P. H., K. Watzke, H. Leser. ME and Miller ,R. (2009) Lipases at interfaces: a review., *Adv Colloid Interface Sci* **147–148**, 237–250.

37. Sangeeta, N. A., B. Rakhi, S. Bhawna, M. Pritish, P. Robin, C. Jesper, B. and Allan, S. (2010) Lipases for use in industrial biocatalysis: Specificity of selected structural groups of lipases, *Journal of Molecular Catalysis B: Enzymatic.* **65**.

38. Evans, P. (2006) Scaling and assessment of data quality, *Acta crystallographica Section D, Biological crystallography.* **62**, 72-82.

39. Kabsch, W. (2010) Xds, *Acta crystallographica Section D, Biological crystallography.* **66**, 125-32.

40. Kabsch, W. (2010) Integration, scaling, space-group assignment and post-refinement, *Acta crystallographica Section D, Biological crystallography.* **66**, 133-44.

41. Long, F., Vagin, A. A., Young, P. & Murshudov, G. N. (2008) BALBES: a molecular-replacement pipeline, *Acta crystallographica Section D, Biological crystallography.* **64**, 125-32.

Tables

Table 1. Kinetic parameters of hydrolysis of *p*-nitrophenyl esters catalyzed by BCE. Kinetic data were measured spectrophotometrically using different concentrations of *p*-nitrophenyl esters at 28°C in 50 mM Tris-HCl pH 8.0 containing NaCl 100 mM and acetone (0.3%).

Substrate	k_{cat} (s^{-1})	K_M (mM)
acetate (C2)	0,621 (± 0.095)	0.873 (± 0.010)
butyrate (C4)	0.264 (± 0.025)	0.049 (± 0.006)
caproate (C6)	0.211 (± 0.020)	0.021 (± 0.005)
caprylate (C8)	0.105 (± 0.004)	0.003 (± 0.001)

Table 2. Hydrolysis of IPG derivatives by BCE. Conditions: substrates [5 mM], BCE 7 mU/mL in Tris-HCl pH 8.0 (50 mM) containing 100 mM NaCl, and DMSO (0.5%). Reactions were monitored by chiral GC.

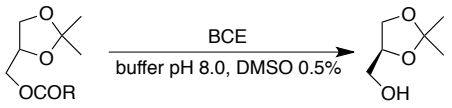

R	**Conversion (%)**	**e.e.$_{substrate}$ (%)**	**e.e.$_{product}$ (%)**	**E**[a]	**Time (h)**
CH_3	46	79 (*S*)	93 (*S*)	67	24
$(CH_2)_2CH_3$	42	70 (*S*)	97 (*S*)	139	1
Ph	49	92 (*S*)	96 (*S*)	163	0.5

[a] E refers to enantiomeric ratio

Table 3. **Data collection, refinement and validation parameters.** Data are shown for the two BCE datasets. [a]$R_{merge} = \sum |I-(I)| / \sum I \times 100$, where I is the intensity of a reflection and *(I)* is the average intensity; [b]$R_{gen} = \sum |F_o-F_c| / \sum |F_o| \times 100$; [c]$R_{free}$ was calculated from 5% of randomly selected data for cross-validation. Values in parentheses represent data belonging to highest resolution shells (Apo-BCE; 1.9-1.94 Å; glycerol-bound BCE 1.8-1.84 Å).

	apo-BCE	BCE+glycerol
Data collection		
Space group	$P6_322$	$P6_322$
Cell dimensions□□		
a, *b*, *c* (Å)	138.6 136.8 83.8	137.6 137.6 83.6
□□□□α□□β,□γ□ (°)	90, 90, 90	90, 90, 90
Resolution (Å)	40-1.9	40-1.8
[a]R_{merge}	0.087 (0.504)	0.113 (0.598)
$I/\sigma I$	26.8 (7.8)	34.9 (8.9)
No. unique reflections	37667 (2359)	43646 (2545)
Completeness (%)	99.8 (99.5)	99.9 (99.8)
Redundancy	19.4 (20.4)	39.1 (37.6)
Refinement		
Resolution (Å)	40-1.9	40-1.8
[b]R_{gen} / [c]R_{free}	21.6/24.3	14.7/16.9
No. atoms:		
Protein	2456	4807
Glycerol	-	18
Chloride ion	-	8
Acetate ion	-	4
Polyethylene glycol	-	6
Water	50	192
B-factors (Å^2):		
Protein	23.9	21.9
Glycerol	-	27.5
Chloride ion	-	44.0
Acetate ion	-	38.7
polyethylene glycol	-	56.2
Water	30	24.1
R.m.s. deviations:		
Bond lengths (Å)	0.014	0.007
Bond angles (°)	1.258	0.856
Ramachandran Plot (%)		
Favored Regions	97.7	98.1
Allowed Regions	100	100

Table 4. *In silico* docking of acetate, -butyrate and -benzoate IPG esters in the active site of BCE. The calculated dissociation constants (Kd) for the S- and R-enantiomers of the acetate, butyrate and benzoate IPG esters are shown, together with the bond length distance between H284 and the ether oxygen which stabilizes the tetrahedral reaction intermediate. Docking was carried out using Autodock 4.2 [43].

Compound	**(R) Kd [μM]**	**(S) Kd [μM]**	**dist. O-H284 (R) (Å)**	**dist. O-H284 (S) (Å)**
Acetate-IPG	139.2	137.6	5.0	5.0
Butyrate-IPG	41.9	43	5.0	4.3
Benzoate-IPG	9.9	7.5	5.7	5.4

Figure Legends

Figure 1. BCE activity towards *p*-nitrophenyl esters. Relative activity refers to the activity in presence of *p*-nitrophenyl caproate (100%) and represents the arithmetic mean and standard deviation (SD) of three measurements.

Figure 2. The crystal structure of apo-BCE and structural comparisons with hMGL. (A) Ribbon secondary structure representation of the crystal structure of apo-BCE. α-helices (blue) and β-strands (grey) and the N- and C-termini are labeled. The lid domain comprising α-helices 5, 6 and 8 is indicated. (B) Secondary structure ribbon representation of apo-BCE (grey) and glycerol-bound BCE (blue). Glycerol and residues F209 and T210 that are orientated diversely in the two structures are shown in sticks. In the glycerol-bound structure, the CZ atom of F209 is located 3.8Å away from the O3 atom of glycerol. In the ligand-free BCE structure the loop moves away from the entrance hole by 3.1 Å. The N- terminus is labeled. This figure was generated using Chimera [31].

(C) View of the interaction between glycerol and BCE residues H113, E284 and a conserved water molecule (W27); hydrogen bonds are indicated by dotted lines. Interaction residues and catalytic triad (S114, H284, D251) residues are labeled and shown in sticks. (D) Superposition of the crystal structures of apo-BCE (blue) and inhibitor-bound hMGL (grey; PDB entry 3JWE, [29]). Structural variations are highlighted in shading. All figures were generated using Chimera [31].

Figure 3. Analysis of the BCE substrate binding site. A) Detailed view of the apo-BCE active site, highlighting the active site tunnel (surface representation); the entrance to the tunnel and the hydrophobic region of the active site are indicated. Hydrophobic residues, the catalytic S114 and the R- and S- enantiomers of butyrate-IPG (sticks) that were *in silico* docked in the cavity are shown; B) *in silico* docking of *p*-nitrophenyl compounds (sticks) with different acyl chains of variable lengths; C2 (pink), C4 (ochre) and C6 (purple); **C)** Illustration of the bond distances between the oxygen and H284 in R- (yellow) and S-(blue) butyrate-IPG. Docking was carried out using Autodock4.2 [43].

Figure 4. Conformational stability of BCE. (A) Thermal unfolding of BCE monitored through far-UV CD at 220 nm as described in the Experimental procedures. The two transitions are labeled T_{m1} and T_{m2}, respectively. Inset: BCE far-UV CD spectrum; (B) the reversibility of the first conformational transition was evaluated by thermal unfolding of BCE, monitored through far-UV CD at 220 nm at protein concentration of 0.1 mg/mL. Native BCE was heated from 20°C to 60°C (blue line) and then cooled down to 20°C The same sample was heated up to 95°C (red line). The two transitions are labeled T_{m1} and T_{m2}, respectively. In this experiment, T_{m2} occurs at higher temperature due to the lower protein concentration.

Figure 1

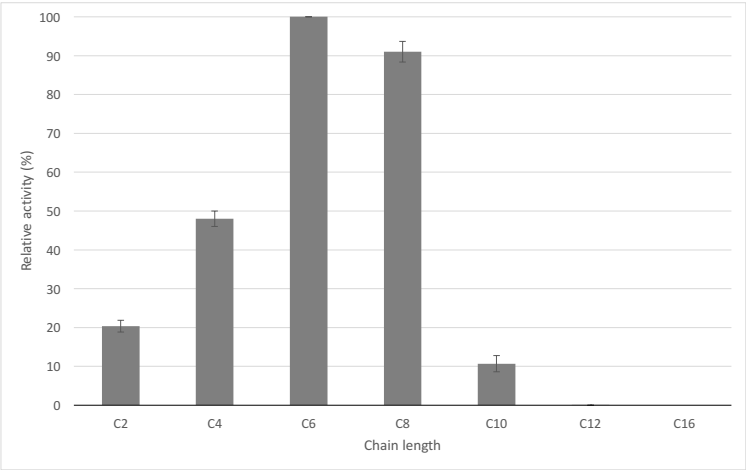
100
90
80
70
60
50
40
30
20
10
0
Relative activity (%)
C2
C4
C6
C8
C10
C12
C16
Chain length

Figure 2A

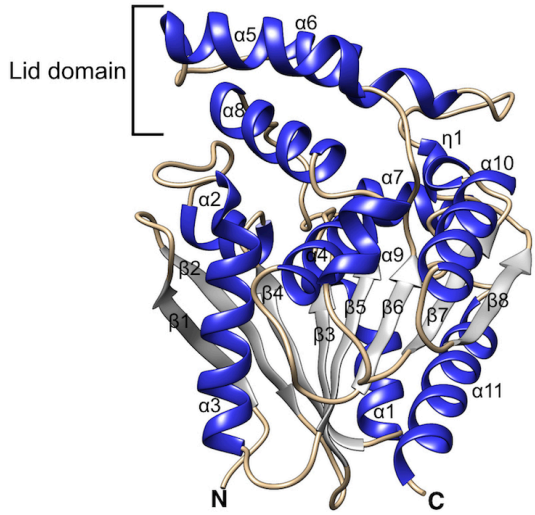

Figure 2B

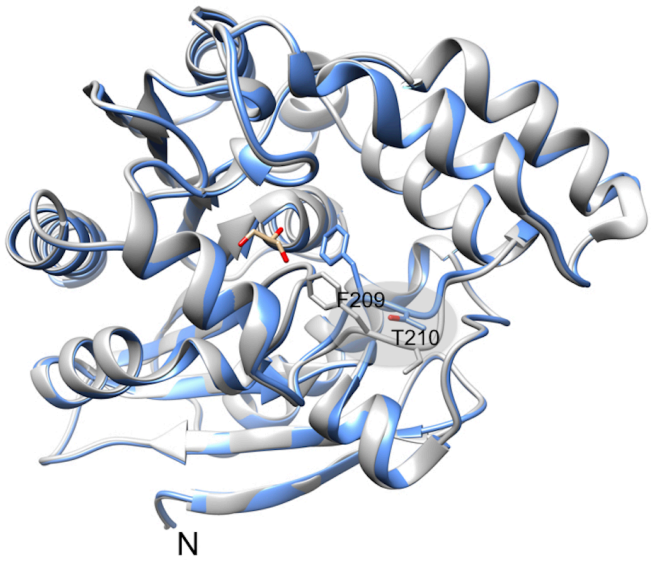

Figure 2C

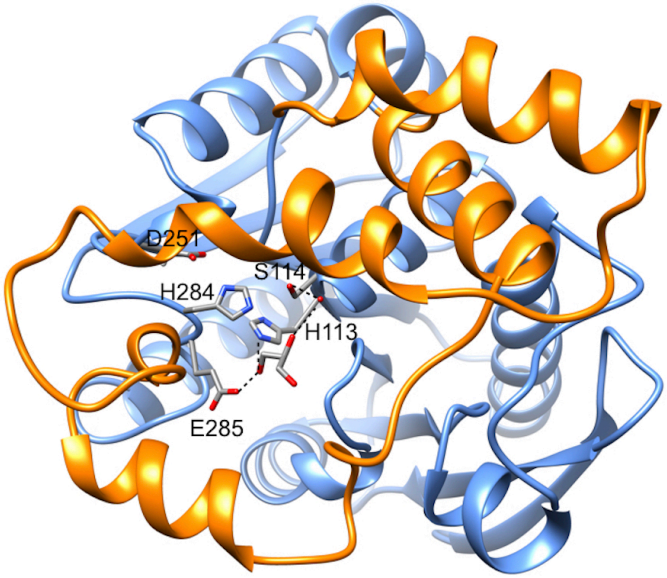

Figure 2D

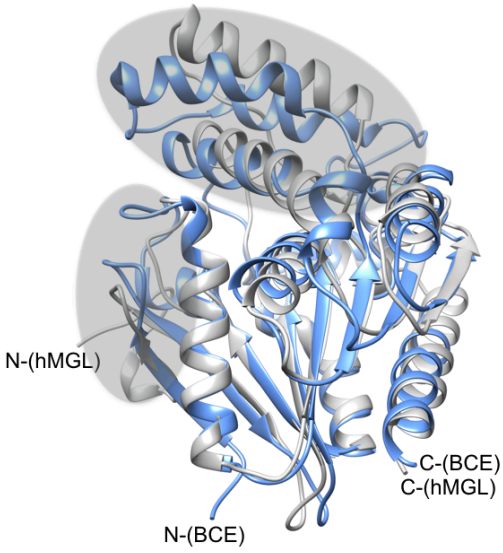

Figure 3A

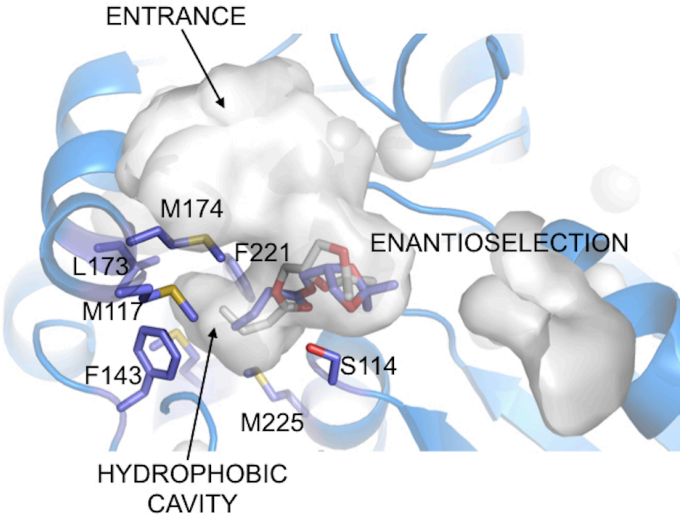

Figure 3B

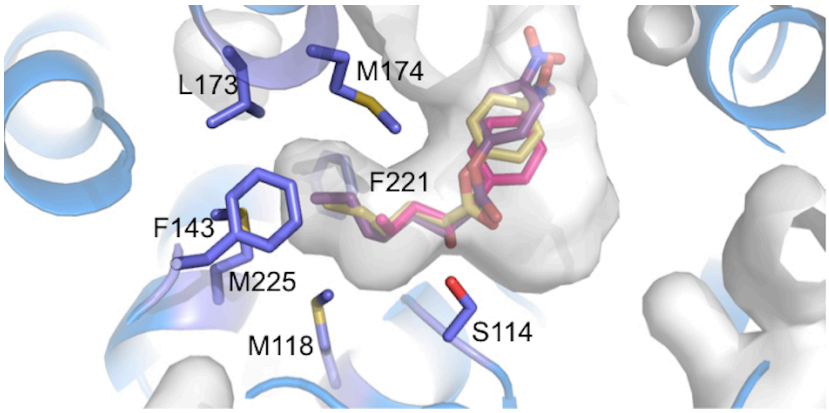

Figure 3C

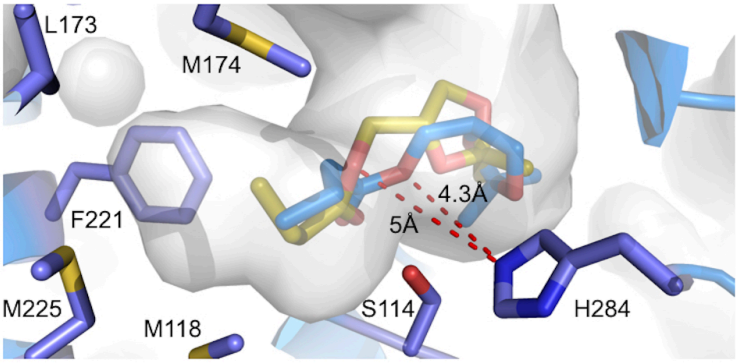

Figure 4A

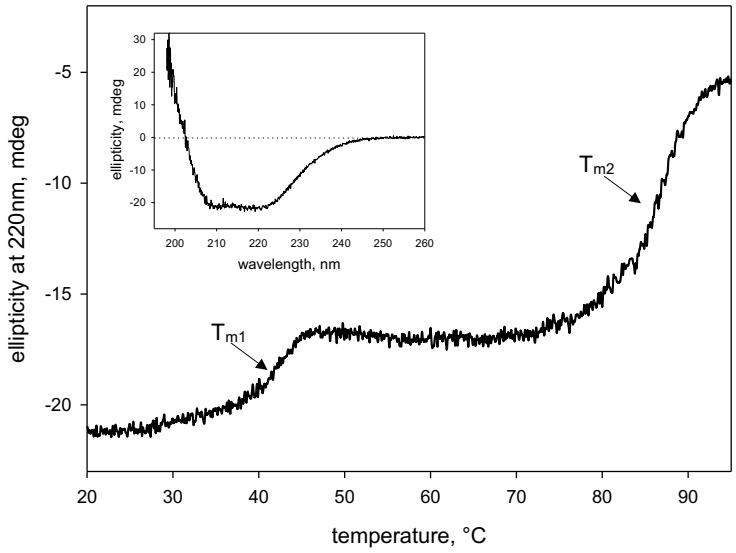

Figure 4B